# APPLICATIONS OF ABERRATION CORRECTED STEM

*Demie Kepaptsoglou[1], Quentin Ramasse[1]*

*[1] SuperSTEM Laboratory, STFC Daresbury, UK,*
*E-mail: dmkepap@superstem.org*

## 1. Introduction

An essential corollary to the exciting instrumentation developments electron microscopy has witnessed over the last decade is the significant increase in detection limits and signal-to-noise ratios achieved on the new generation aberration-corrected microscopes, which provide improved data collection ability and greater flexibility. The development of so-called 'gentle', dose-controlled Scanning Transmission Electron Microscopy (STEM) techniques [1], for instance, has been particularly beneficial for the field of two-dimensional materials: examples of graphene [2,3] demonstrate how these structures can be imaged directly at atomic resolution with annular dark field (ADF) imaging while single atom impurities or defects can be chemically fingerprinted using spectroscopy [3-5]. In addition, the wealth of complementary analytical signals available from a single experiment provide unprecedented insights into the properties of materials.

In this paper some applications of aberration corrected STEM combined with Electron Energy Loss Spectroscopy (EELS) are presented. They include direct evidence of interfacial charge transfer in solid-oxide fuel cell anodes, high-precision chemical analysis and structural determination of functional oxides and detailed quantum effects in Si-based photovoltaic thin films.

## 2. Probing the Bonding and Electronic Structure of Single Atom Dopants in graphene

In recent years graphene has been dubbed the "miracle" material, generating a true research frenzy: from production methods and doping techniques, to physical properties and novelty applications. Due to its very high carrier mobility, graphene is very attractive for electronic applications [6]. However it is an excellent conductor – or a 'zero bandgap' semiconductor - which so far inhibits its use in device applications. It is thought that the introduction of minute structural variations, such as defects or ad-atoms will have a dramatic effect on the electronic configuration, such as opening of the bandgap [6], and therefore graphene's properties as a functional material. As these structural variations occur at the atomic level, it is essential to study graphene one atom at a time.

In this example we show how a combination of STEM, EELS, and ab initio calculations can be used to reveal striking electronic structure differences between two distinct single substitutional Si defect geometries in graphene (Figure 1); namely trivalent and tetravalent Si. Optimised acquisition conditions on a Nion UltraSTEM100 dedicated STEM instrument, allow for exceptional signal-to noise levels in the spectroscopic data. The near-edge fine structure can be compared with great accuracy to simulations and reveal either an *sp3*-like configuration for a trivalent Si or a more complicated hybridized structure for a tetravalent Si impurity (Figure 1c).
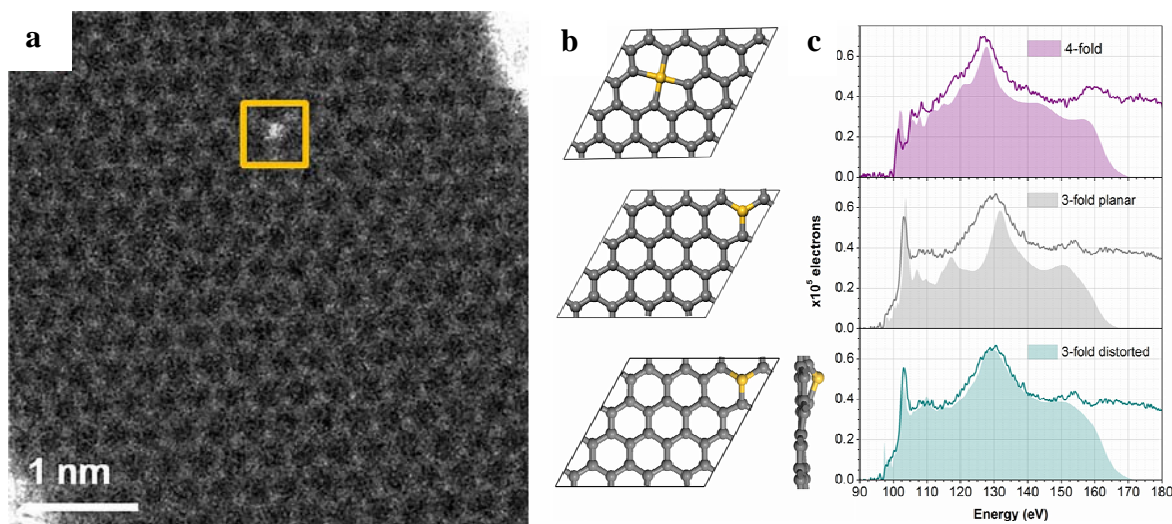
Figure 1a ). *HAADF image (raw data) of a Si atom substituted within a single layer graphene Sheet, b) Models of tetravalent and trivalent substitutional Si atoms within a single-layer graphene sheet. The atomic positions were optimized using DFT calculations. (c) Comparison between the experimental spectra (solid lines) after background subtraction using a decaying power law, and the spectra calculated by DFT using the models shown in (a) (shaded areas).*

## 3. Electron Microscopy Study of interfaces of Proton Conducting Fuel Cell Anodes

In the race for clean and efficient production of energy, solid state fuel cells emerge as cutting edge technology with very promising results. High-temperature proton conductors are oxides with oxygen deficiency in the form of dilute oxygen vacancies, where protons dissolve as hydroxide defects in the oxide at the expense of the vacancies. Acceptor-doped proton conducting oxides, such as Ca-doped orthoniobates have shown remarkable conduction properties and chemical stability and thus show great potential in their employment as components for solid state fuel cells [7, 8]. To a large extent the functionality and overall efficiency of fuel cells is dependent on the nature of oxide/oxide and metal/oxide interfaces in its electrodes, since the current is often limited by the conductivity of the grain boundaries and by electrode kinetics. In particular, the mobility of charge carriers across or along interfaces can be affected by the presence of electrical charging and oxygen vacancies as a result of doping, local structural changes at the interface or the formation of interfacial precipitation layers [9].

The TEAM 0.5 instrument, a modified double-corrected FEI Titan[3] microscope [10], was used to study the structural and chemical characteristics of the interfaces between Ni and $LaNbO_4$ (LMO) grains in $Ni-LaNbO_4$ cermets, a candidate material for fuel cell anodes [7, 11]. Electron energy loss spectroscopy (EELS) was used to investigate the precipitation of dopants or formation of secondary phases at the $Ni/LaNbO_4$ boundaries. Spatially resolved linescans across the boundaries, showed the absence of reaction or interdiffusion layers at the interface.
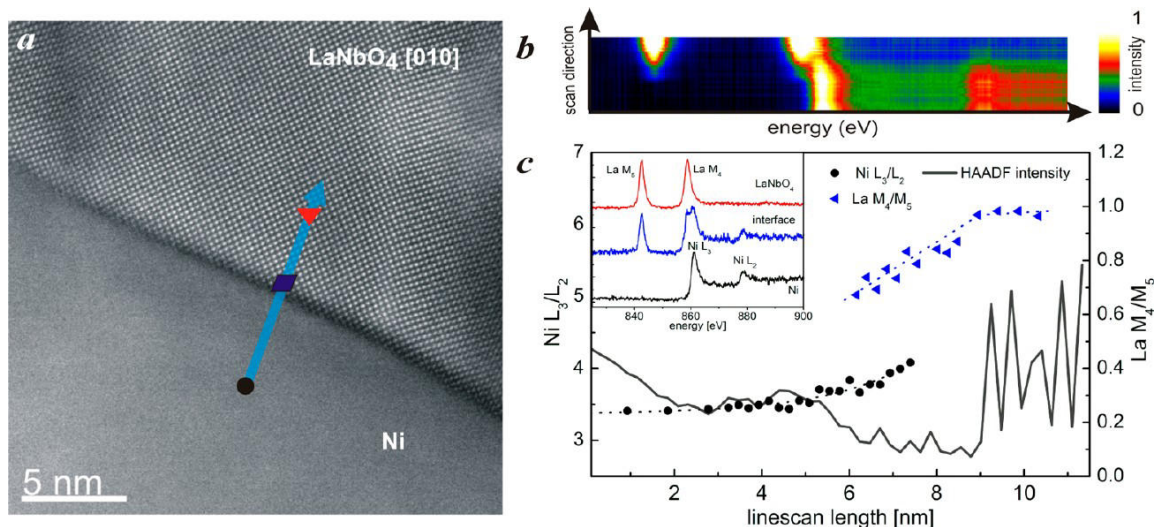
Figure 2. *(a) HAADF STEM image of the Ni/LNO interface and the path of the EELS linescan; (b) raw EELS spectrum image of the La $M_{4,5}$ and Ni $L_{2,3}$ core loss edges, showing the La $M_5$ and Ni $L_3$ overlap; (c) Ni and La white line ratio values plotted as a function of position, together with the intensity of the HAADF image along the linescan.*

The experimental results revealed a drastic change of the electronic structure when moving from the bulk to the interface region, quantified by a significant change of the EELS white line ratios of Ni and La, respectively. Despite the consistent increase in the Ni oxidation state, the presence of a Ni oxide layer was excluded. Thus, the interface was shown to be chemically abrupt, leading to the assumption that bonding occurs between Ni and the O of the LaNbO$_4$ phase. The experimental results were compared to DFT calculations of a defect-free model of the Ni/LNO interface. They demonstrated direct chemical bonding and a significant exchange of electrons from Ni to La and O at the interface layer. This charge transfer was quantified by theoretical calculations in very good agreement with the experimental findings. These results show how atomic-scale analytical electron microscopy measurements coupled with ab initio calculations can be used to characterize directly the nature of the chemical bonds forming across a metal/oxide interface in a complex cermet material. Such understanding is essential for further design and optimization of solid-oxide fuel cells. [11].

## 4. Quantum Confinement in Germanium Quantum Dots Observed by Electron Energy-Loss Spectroscopy

Quantum dots (QDs) embedded in dielectric matrices such as silicon dioxide, have attracted a great deal of attention, due to their tailorable electronic and optical properties for a wide range of optoelectronic and solar cell applications [12]. It is well-demonstrated that the electronic structures of the valence band and the conduction band are strongly modified in these QDs [13]. In order to tailor these systems for optoelectronic applications, it is extremely important to understand how their properties evolve as a function of QD size and structure.
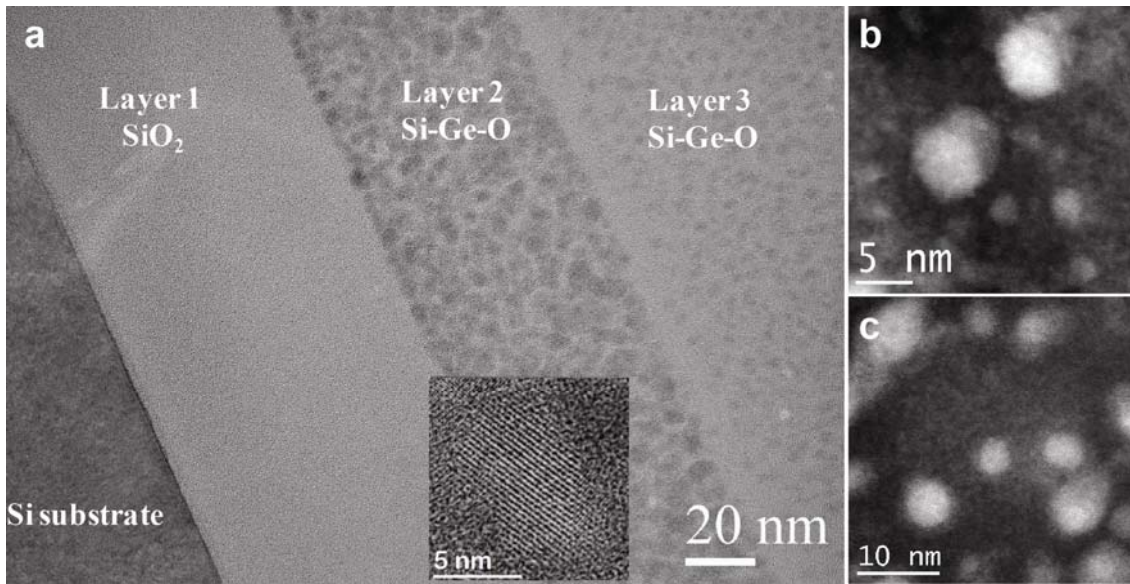
Figure 3 *(a) Cross-sectional high-resolution transmission electron microscope image showing the sample structure: layer 2 has a higher density and bigger grain size of Ge QDs (5–10 nm) than layer 3 (3–5 nm). The inset shows clear lattice fringes of a Ge QD in layer 2. (b) and (c) High-angle annular dark-field (HAADF) STEM images of Ge QDs in layer 2 and 3, respectively.*
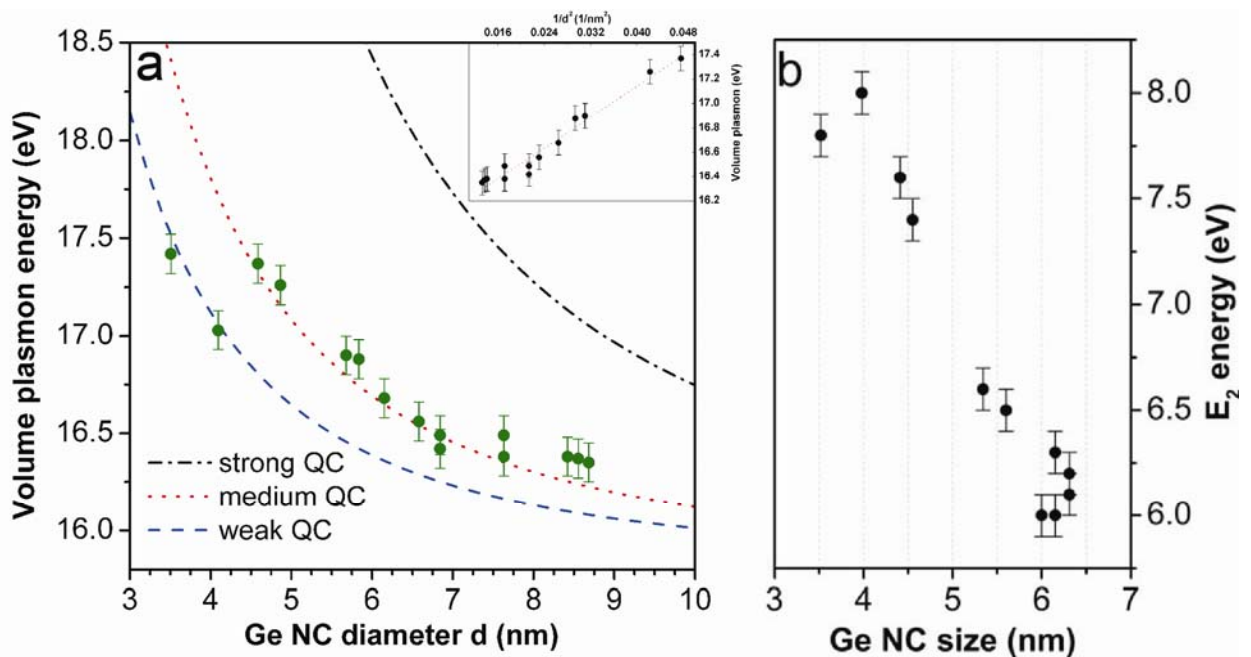


Figure 4. *(a) QD size dependence of the Ge volume plasmon energy, extracted from low loss EELS spectra acquired at the cores of individual Ge QDs. The dotted-dashed, dotted, and dashed curves show the theoretically predicted $E_P \sim 1/d^2$ relationship in three different regimes: strong, medium, and weak quantum confinement, respectively. The inset shows the data fitting for QDs with diameters > 4 nm. (b) The blue shift of $E_2$ transitions with decreased QD size.*

24

In this example we present how STEM EELS could be used in order to directly observe quantum confinement (QC) effects in within individual embedded nanostructures, in size-controlled Ge QDs in a silicon dioxide thin film matrix system (Figure 3) [14]. In EELS, quantum confinement effects are manifested by changes in the volume plasmon and interband transition energies of individual Ge QDs, with respect to their size and structure. Changes in the band gap structure of the QDs arising from QC can be observed by shifts to higher energies (blue-shift) of volume plasmon and interband transition energies with decreasing QD size. The shifts in the plasmon energies (Figure 4a) and the $E_2$ interband transition (Figure 4b), acquired within individual QDs, are showing a direct correlation to their size and structures (Figure 3). The volume plasmon energy $E_p$ (eV) is related to the size d (nm) of Ge QDs by $E_p = 15.87 + 31.58/d^2$ (see the inset in Figure 2a), which gives an estimated effective mass $\mu = 0.57m_0$, where $m_0$ is the electron rest mass, consistent indeed with a so-called medium confinement model.

In the very low-loss region of the EEL spectra, an apparent blue shift of the $E_2$ interband transition peak up to 2 eV and a strong reduction in the oscillator strength were measured for the QDs in the size range of 4–6 nm. This indicates that for this small size range there is a transition to a QC regime where the band structure and the density of states are modified dramatically. Crucially, the observed variation of Ge band structure via engineering of the QD size, structure and the matrix composition suggests a practical way of tuning the efficiency of optoelectronic devices.

## 5. High-precision chemical analysis and structural determination of functional oxides by STEM-EELS

Chemical doping of functional complex oxides is perhaps the most widespread means of tailoring their physical properties, which crucially depend on the materials' atomic arrangements at the sub-angstrom scale. Minute changes in their composition can dramatically alter the local atomic configuration and thus transform the physical properties of these oxides. As these effects are often too local to be fully understood through bulk characterization methods, due to the presence of point or extended defects for instance, STEM EELS has become a ubiquitous tool in their study. When these techniques are combined with advanced statistical image analysis [15] it is possible to determine statistically the chemical distribution of the different sites in these structures across a range of compositions and to relate those to accurately measured small local atomic displacements generated by these compositional changes.

In this example we present a combination of STEM/EELS and statistical image analysis in functional complex oxide systems with varying cation contents. The thermoelectric properties of the perovskite system $(1-x)SrTiO_3-xLa_{2/3}TiO_3$ can be fine-tuned by adjusting the La/Sr ratio, *i.e.* by varying x. HAADF imaging in an aberration-corrected STEM revealed that in the La-rich side of the compound series there are two distinct A lattice sites with strikingly different column intensities (Figure 5a). In combination with 2D EELS mapping it is revealed that one of the two A sites (site A1) is fully occupied by La, while the other (A2) exhibits either a shared occupancy of Sr or La vacancies. Further analysis of the EELS data as well as statistical analysis of the image intensities is used to determine the cation concentration at La-deficient sites. The structural variations derived from image and chemical map analysis are in turn related to fine structure changes in the EELS maps, notably for the Ti $L_{2,3}$ edge (Figure 5b).
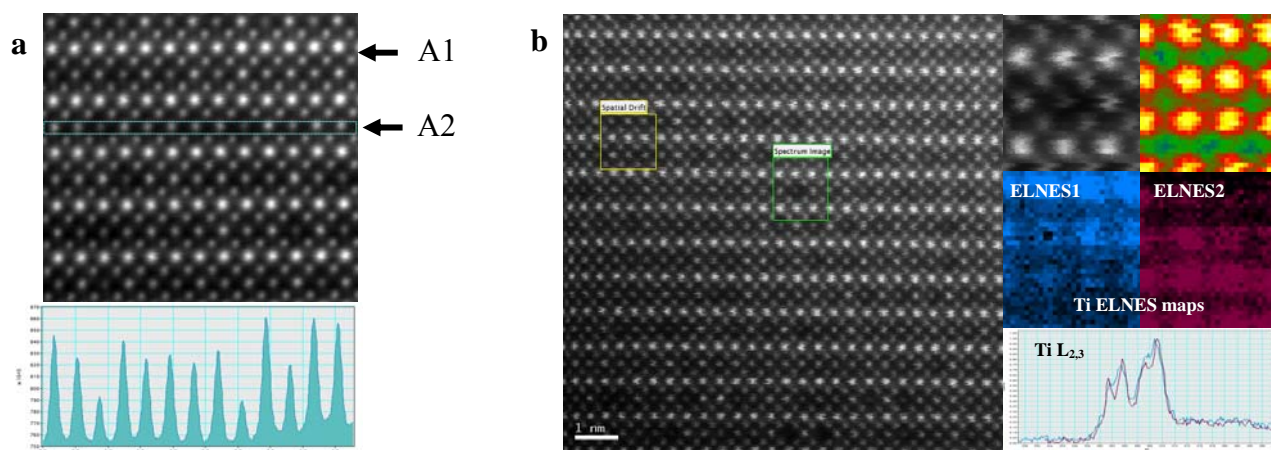
Figure 5. *a) Stack-averaged HAADF STEM image showing two distinct A sites in $La_{0.6}Sr_{0.1}TiO_3$ and intensity profile of the A2 site, (b) HAADF STEM survey image of a La-vacancy in the A2 cation site, corresponding atomically-resolved Ti and Ti ELNES maps.*
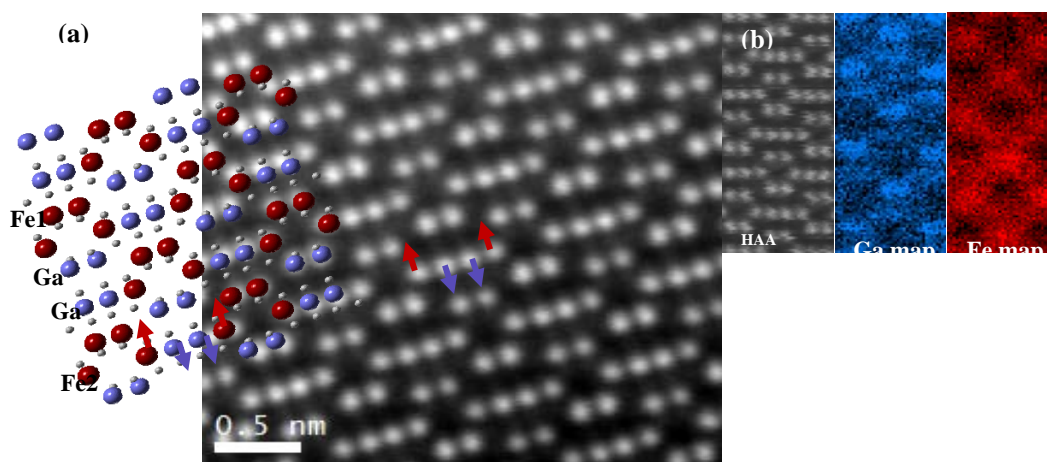


Figure 6. *(a) Ball and stick model of gallium ferrite and stack-averaged HAADF image of the $Ga_{1.2}Fe_{0.8}O_3$ composition and (b) atomically resolved Fe map.*

Furthermore, the magneto-electric oxide gallium ferrite $Ga_{1-x}Fe_xO_3$, whose spontaneous polarization is dependent on the distortions caused by the structural asymmetry of the cation sites [17], provides another example of combined EELS and image analysis methodology. Analysis of the HAADF image intensities as well as detailed 2D EELS mapping is used to demonstrate that in the intermediate compositions cation intermixing occurs mainly in the Fe2 and Ga2 sites (Figure 6). Advanced image analysis is used to determine the respective displacement of the Fe2 and Ga2 sites with respect to the atomic composition.

**References:**
[1]     O. L. Krivanek *et al.*, Ultramicroscopy, **110**, 935−945, (2010)
[2]     J.C. Meyer *et al.*, Nano Lett., **8**, 3582, (2008)
[3]     Q. M. Ramasse *et al.*, Nano Lett., DOI: 10.1021/nl304187e, (2013)
[4]     T. C. Lovejoy et al., Applied Physics Letters, **100**, 154101, (2012)
[5]     W Zhou *et al*, Phys. Rev. Lett., **109**, 206803, (2012)
[6]     M.Y. Han et al., Phys Rev Lett, **98,** 206804, (2007)
[7]     R. Haugsrud and T. Norby, Nature Materials, **5**, 193, (2006)
[8]     H. Fjeld *et al.*, Solid State Ionics, **181**, 104, (2010)
[9]     X. Guo and R. Waser, Prog. Mater. Sci., **51**, 151, (2006)
[10]    C. Kisielowski et *al.*, Microscopy and Microanalysis **14**, 454, (2008)
[11]    D.M. Kepaptsoglou *et al.*, Chem. Mater., **24**, 4152, (2012)
[12]    L. Pavesi and R. Turan in "*Silicon Nanocrystals*", ed. L. Pavesi (Wiley-VCH, Berlin,), p. 1.
[13]    G. Conibeer in "*Silicon Nanocrystals*", ed. L. Pavesi (Wiley-VCH, Berlin), p. 555.
[14]    P. D. Nguyen *et al.*, Phys. Rev. B., **86**, 245316, (2012)
[15]    M.C. Sarahan *et al*., Ultramicroscopy **111,** 251, (2011)
[16]    A Kinaci *et al.*, Physical Review B, **82,** 155114, (2011)
[17]    A. Roy *et al*., J. Phys.: Condens. Matter **23,** 325902, (2011)